Journal of the European Ceramic Society xxx (xxxx) xxx

Contents lists available at ScienceDirect

Journal of the European Ceramic Society

journal homepage: www.elsevier.com/locate/jeurceramsoc

Book-Shaped All-in-One Piezo-Triboelectric Energy Harvester Module with Enhanced Current Characteristics As an Eco-Friendly Energy Source

Sang Hyun Ji [a,b], Wooyoung Lee [b,*], Ji Sun Yun [a,*]

[a] Energy & Environmental Division, Korea Institute of Ceramic Engineering and Technology, 101, Soho-ro, Jinju, 52851, Republic of Korea
[b] Department of Materials Science & Engineering, Yonsei University, Seoul, 03722, Republic of Korea

ARTICLE INFO

Keywords:
Piezoelectric
Triboelectric
Nanofiber
Flexible
Energy harvesting

ABSTRACT

A book-shaped all-in-one energy harvester module with a piezo-triboelectric hybrid structure as a next-generation eco-friendly energy source was manufactured based on flexible piezoceramic nanofibers with enhanced current characteristics obtained by controlling the added amount of carbon black (CB). To prepare flexible piezoceramic nanofibers with favorable current properties, $0.78Bi_{0.5}Na_{0.5}TiO_3-0.22SrTiO_3$ (BNT-ST) piezoelectric ceramics were composited with CB, a highly conductive material, and then electrospun with a poly (vinylidene fluorideco–trifluoroethylene) polymer. The prepared CB/BNT-ST nanofibers were modularized into piezoelectric energy harvester modules (PEHMs) with interdigitated electrodes, yielding an improved output performance with a high voltage of 10.1 V and high current of 2.02 nA. A book-shaped triboelectric energy harvester module (TEHM) was manufactured with polydimethylsiloxane on one side and the CB/BNT-ST nanofibers on the other side, affording an improved output performance with a high voltage of 391 V and high current of 130 μA. A book-shaped all-in-one hybrid energy harvester module (HEHM) was then manufactured by fitting PEHMs at both ends of the book-shaped TEHMs. As a result of optimizing the output performance by connecting HEHM multiple layers, a high voltage and current of 1043 V and 579 μA were observed, respectively, and charging of a 1.0 μF capacitor was completed in 25 s. Furthermore, in simulated energy harvesting experiments using the all-in-one HEHM, LED light bulbs were clearly illuminated in real time, and an electronic calculator was operated without charging. This work suggests the application potential of the all-in-one HEHM as the next generation of eco-friendly flexible energy sources.

1. Introduction

Renewable and sustainable energy sources continue to attract attention as solutions to problems like the depletion of existing energy sources and the consequences of environmental pollution such as global warming. [1] Many researchers have focused on eco-friendly energy sources such as solar power [2], hydroelectric power generation [3], and tides [4] as new energy sources to replace existing ones. However, since they involve large-scale energy produced in large-scale facilities, these new energy sources are limited in that they are difficult to apply to wearable small electronic devices for personal health management, biomonitoring, and environmental monitoring. Therefore, collecting and utilizing unused mechanical energy from the surroundings with materials such as piezoelectrics [5] and triboelectrics [6] has begun to attract attention as an eco-friendly energy source for wearable electronic devices owing to the advantages of miniaturization, efficiency, and simplicity. Research has been actively conducted to improve the performance of piezoelectric and triboelectric materials by optimizing various types of module structures such as piezoelectric [7], triboelectric [8] and piezo-triboelectric hybrid nanogenerators [9–11]. However, there are still limitations in their output performance, especially in terms of output current, for application in the actual electronics industry.

Several notable organic and inorganic piezoelectric materials, including lead zirconate titanate (PZT), [12,13] barium titanate ($BaTiO_3$), [14,15] and poly(vinylidene fluorideco-trifluoroethylene) (P(VDF–TrFE)) [16,17] have been studied for use in piezoelectric nanogenerators. Although these inorganic materials generally have more favorable piezoelectric properties than organic materials, various problems such as their durability have been raised owing to their inherent properties, such as their brittleness and stiffness. On the other hand, ferroelectric polymers have excellent flexibility, which can overcome the brittleness and stiffness of inorganic materials, but have

* Corresponding authors.
E-mail addresses: wooyoung@yonsei.ac.kr (W. Lee), susubin@kicet.re.kr (J.S. Yun).

https://doi.org/10.1016/j.jeurceramsoc.2021.11.047
Received 22 August 2021; Received in revised form 24 October 2021; Accepted 22 November 2021
Available online 24 November 2021

unfavorable piezoelectric properties. To overcome the disadvantages of inorganic and organic piezoelectric materials and to maximize their advantages, various organic–inorganic composite technologies have been studied [18,19]. Nevertheless, energy harvesting modules based on piezoelectric composites of polymers and ceramics produce very low output voltages and currents, making it difficult to use them to operate small electronic devices [20,21]. To produce more power, most researchers have improved the output voltage by developing piezo-triboelectric hybrid nanogenerators, [22] but there are still limited output currents as low as tens of nanoamperes.

In this study, an all-in-one hybrid energy harvester module (HEHM) was manufactured by fitting piezoelectric energy harvester modules (PEHMs) at both ends of book-shaped triboelectric energy harvester modules (TEHMs) and connecting multiple layers. The output voltages and currents of the individual PEHMs and TEHMs within the all-in-one HEHMs were measured independently and integrally. To improve the output current, the $0.78Bi_{0.5}Na_{0.5}TiO_3-0.22SrTiO_3$ (BNT-ST) piezoelectric ceramics were composited with carbon black (CB), which has a high conductivity, [23] to prepare flexible piezoelectric nanofibers by an electrospinning process. The nanofibers showed enhanced output current properties upon controlling the CB content and were applied in both the PEHMs and TEHMs. Because CB has many free electrons owing to its small particle size and high electrical conductivity, a high current can be produced inside the PEHM piezoelectric material to maximize the output voltage and current; at the same time, the surface energy of the friction material in the TEHM can be controlled to maximize the output voltage and current [24]. In the book-shaped all-in-one HEHM, as the book form closes and then opens, energy is generated from each individual PEHM and TEHM, and the output power can be maximized by increasing the number of layers. Furthermore, the book-shaped all-in-one HEHM can be opened and closed at a uniform speed and force by fixing it on a bending machine, which has the advantage of allowing for quantitative evaluation of the output characteristics. The book-shaped all-in-one HEHM showed a high voltage of up to 1043 V and current of 579 μA and a high durability, with the output voltage and current remaining almost the same even after bending operations were performed more than 10,000 times.

2. Experimental

2.1. Materials

High-purity bismuth(III) oxide (Bi_2O_3), sodium carbonate (Na_2CO_3), titanium oxide (TiO_2), and strontium carbonate ($SrCO_3$) were purchased from Kojundo Chemical, and carbon black (CB) was purchased from US Nano. P(VDF–TrFE) with a composition of 75/25 mol% was purchased from Measurement Specialties, and PDMS (Sylgard 184) was purchased from Dow Corning. The 99.5% *N,N*-dimethylformamide (DMF) and 99.995% acetone solvents used in the experiments were purchased from Sigma-Aldrich and Daejeong Chemical, respectively.

2.2. Synthesis of piezoelectric ceramics

CB/BNT-ST piezoelectric ceramics were prepared by a conventional solid-state reaction method. A two-step calcination process was employed to obtain good uniformity and crystal properties. First, all powders except CB were prepared according to the stoichiometric composition, ball milled for 24 h with absolute ethanol, and dried for 24 h at 80 °C in air. The dried powder was calcined at 800 °C at a rate of 5 °C/min for 2 h. Subsequently, different amounts of CB were added to the calcined BNT-ST powder, followed by ball milling in absolute ethanol for 24 h and finally drying in air at 80 °C for 24 h. The dried powder was sieved through a mesh to control the particle size to less than approximately 100 μm. The controlled powder was pressed into a 12 mm diameter disk at a pressure of 200 MPa by adding a PVA binder, and the manufactured disk was sintered at 1150 °C for 2 h. The CB/BNT-ST ceramic disc samples were then poled under an electric field of 20 kV/cm in silicon oil at 70 °C for 30 min.

2.3. Fabrication of HEHM

To manufacture the HEHMs, PEHMs and TEHMs were first manufactured. For PEHM fabrication, [25] the piezoelectric ceramic powders with different CB contents were added to a P(VDF–TrFE) solution at a concentration of 60 wt% (P(VDF–TrFE): DMF: acetone = 2:5:5), and the mixture was vigorously stirred at 1500 rpm for 24 h to prepare a homogeneous precursor solution. The prepared homogeneous precursor solution was filled in a 12 mL plastic syringe connected to a 21 G metal needle, and the metal needle was connected to a voltage power supply to perform an electrospinning process for nanofiber preparation. For electrospinning, a high voltage of 10–15 kV was applied to the metal needle, and the precursor solution was discharged for 8 h at a rate of 1 mL/h using a syringe pump. The electrospun CB/BNT-ST nanofibers were collected in a cylindrical drum collector rotating at 1500 rpm at room temperature and 20%–40% humidity, and the distance from the needle tip was maintained at 10 cm. For fabrication of the PEHMs with dimensions of 1 cm (width) × 5 cm (length), the CB/BNT-ST nanofibers and the IDE electrodes with electrode width of 0.10 mm and electrode spacing of 0.20 mm were laminated by the warm isostatic press process at 70 °C and 80 bar for 30 min. The manufactured module was then subjected to a polarization process at 1 kV for 1 h.

For fabrication of the TEHMs, PDMS and a curing agent were mixed at a mass ratio of 10:1 wt%, and an aluminum electrode was attached on one side and a micropatterned substrate to the other side, followed by curing at 80 °C for 1 h in a vacuum atmosphere. [22] Subsequently, the cured PDMS was separated from the micropatterned substrate to fabricate one side of the TEHM. The other side of the TEHM was prepared from CB/BNT-ST nanofibers electrospun for 5 h on an SUS substrate used as an electrode, and each of the prepared sides was fixed into a book shape with polyester tape. A PEHM was fixed at both ends of the book-shaped TEHM to manufacture the book-shaped all-in-one HEHM, and single all-in-one HEHMs were connected in multiple layers.

2.4. Characterization

The crystal structures of the CB/BNT-ST piezoelectric ceramics were analyzed using XRD (max 2200 V, Rigaku Corporation), and the microstructure was analyzed by FE-SEM (JSM-6700 F, JEOL). The *P–E* hysteresis loops and *S–E* curves of the CB/BNT-ST piezoelectric ceramics were measured using a ferroelectric test system (Radiant P-LC-K). The piezoresponse hysteresis loops of the CB/BNT-ST piezoelectric ceramics and CB/BNT-ST nanofibers were studied using a PFM device (A100-AFM, A. P. E. Research) under an applied AC voltage with an amplitude of 1.5 V and frequency of 520 kHz. The temperature-dependent dielectric properties of the CB/BNT-ST piezoelectric ceramics were measured using an impedance analyzer (HP4284A, Agilent Tech. Inc.). The output voltages and currents of the modules according to bending movements applied by a bending machine (CERATORQ) were recorded with an oscilloscope (Tektronix, DPO 2012 B) and digital power meter (Yokogawa, WT 310), respectively, at the different load resistances from 1.5 MΩ to 5 MΩ by connecting a potentiometer (Hanil Electronics, RV24YN B-3). The values of output voltages and currents at the load resistance with the maximum output power were finally recorded.

3. Results & discussion

3.1. Optimization of CB content of CB/BNT-ST piezoelectric ceramics

The crystal structure of the CB/BNT-ST ceramics was studied according to the CB content, as shown in Fig. 1. The XRD peak of the CB powder at $2\theta = 20°–30°$ was very broad, which is typical of CB. [26] On the other hand, the diffraction peak of the pure BNT-ST ceramic was

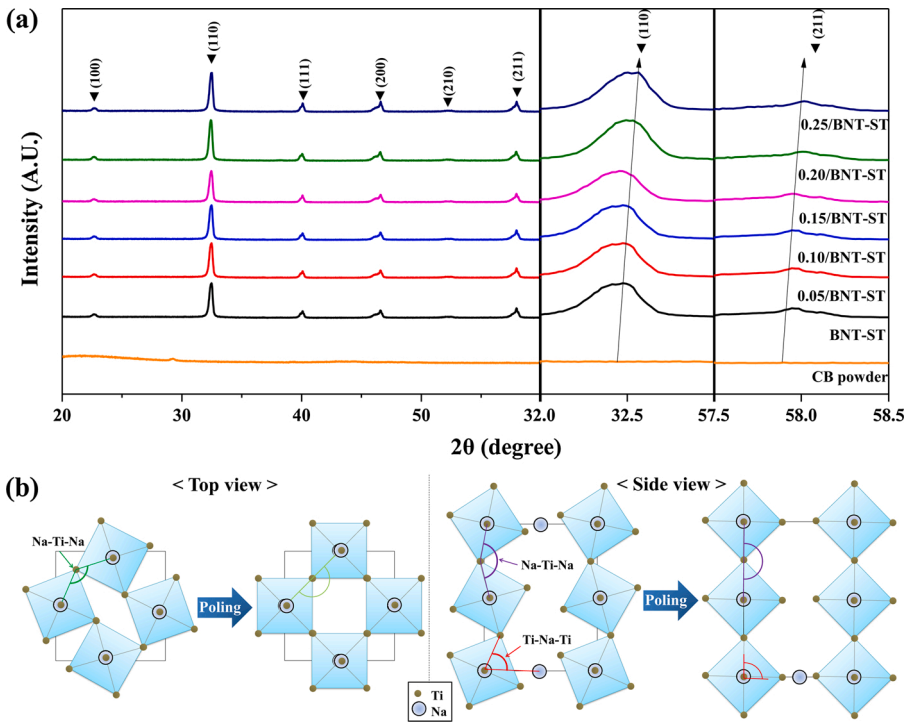

Fig. 1. (a) XRD patterns of the CB/BNT-ST ceramics with different CB contents. (b) Schematic illustrations of the ideal alignments of Na-centered Ti octahedra with perfect poling: top view showing the changes in the Na–Ti–Na bonding angle in the ac-plane and side view showing the changes in the Na–Ti–Na and Ti–Na–Ti bonding angles along the b-axis.

sharp and crystalline, and a high-quality perovskite phase was observed [27]. In the XRD patterns of the CB/BNT-ST ceramics with different CB contents, although the XRD peak of CB could not be clearly observed because of the small amount of added CB, the (110) peak at 32°–33 ° and (211) peak at 57.5°–58.5 ° of BNT-ST shifted slightly to higher angles as the CB content increased. The lattice parameters and average grain sizes in Table S1 and the bonding angles in Table S2 were mathematically calculated based on the XRD patterns in Fig. 1(a) according to Bragg's law. The lattice parameter usually changes depending on shifts in the diffraction peaks, [28] and as the CB content increased, the lattice size, volume, crystallite size, and grain size of CB/BNT-ST gradually increased. Furthermore, the tetragonality (c/a) given in Table S1 increased with CB content, which means that the perovskite percentage of the CB/BNT-ST ceramics increased with CB content, allowing for better piezoelectric properties. [29] In other words, the lattice structure of CB/BNT-ST is affected by the addition of CB. Fig. 1(b) shows schematic illustrations of the ideal alignment of Na-centered Ti octahedra in the lattice structure of the BNT-ST ceramic with perfect poling. The Na–Ti–Na angle in the *ac*-plane and the Ti–Na–Ti and Na–Ti–Na angles along the *b*-axis gradually increased with CB content, as shown in

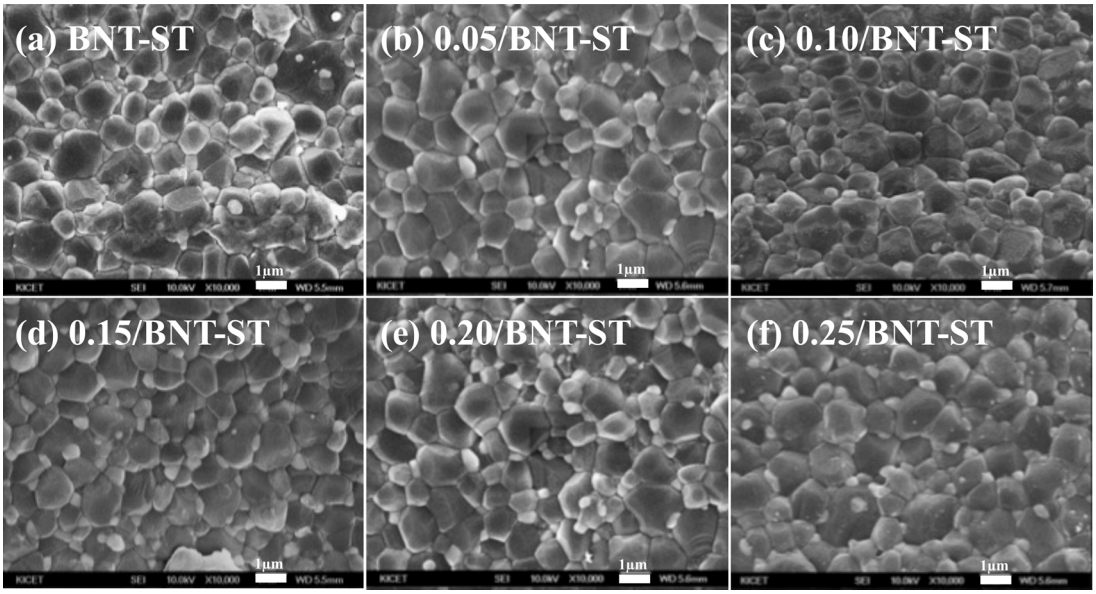

Fig. 2. FE-SEM micrographs of the CB/BNT-ST composites with different CB contents: (a) BNT-ST, (b) 0.05/BNT-ST, (c) 0.10/BNT-ST, (d) 0.15/BNT-ST, (e) 0.20/BNT-ST and (f) 0.25/BNT-ST.

Table S2, which is expected to contribute to the effective polarization of the piezoelectric ceramic.

The microstructure of CB/BNT-ST with different CB contents was observed by SEM after sintering at 1150 °C for 2 h, as shown in Fig. 2. Although CB contents of 0–0.25 wt% were added, the grain structure and grain boundary of the ceramic remained unbroken and well maintained for all samples. The graphs in Fig. S1, however, show that the grain size of CB/BNT-ST gradually increased with CB content, and a maximum relative density of 99.99% was observed for the 0.10/BNT-ST ceramic (0.10 wt% CB content). Since the grain size of the piezoelectric ceramics also increased with CB content, the relative density gradually increased by CB initially filling the spaces between grains. However, when excess CB was added, the relative density decreased due to void reformation. This is believed to be because CB reportedly acts as a binder to induce grain growth during the sintering process, leading to homogeneity and defects in the samples. [29] Furthermore, these changes in grain size and relative density according to CB content are expected to have a significant influence on the piezoelectric performance. [30]

The temperature dependence of the dielectric constant and dielectric loss of the CB/BNT-ST ceramics with different CB contents was investigated at frequencies of 1, 10, 100, and 1000 kHz, as shown in Fig. 3. The dielectric constant, which indicates the poling efficiency, results from permanent dipole motion within a piezoelectric system. [23] There are two successive dielectric anomalies in the temperature dependence of the dielectric constant because of the relaxor nature of BNT-based materials [31]. The first dielectric anomaly is located at the temperature T_s (approximately 110–130 °C at 1 kHz) and is accompanied by an obvious frequency dispersion, which is caused by thermal evolution of the R3c and P4bm polar nano-region mixture. The second dielectric anomaly is located at T_m (approximately 178–191 °C at 1 kHz) and is also known as the Curie temperature (T_C). The dielectric constant and T_m increased with CB content because the electrical conductivity of the CB/BNT-ST ceramics was improved by the addition of a small amount of conductive additive (CB). Furthermore, as the CB content increased, the shoulder at T_s gradually disappeared due to the increased number of CB particles on the surface of the BNT-ST ceramic particles minimizing the

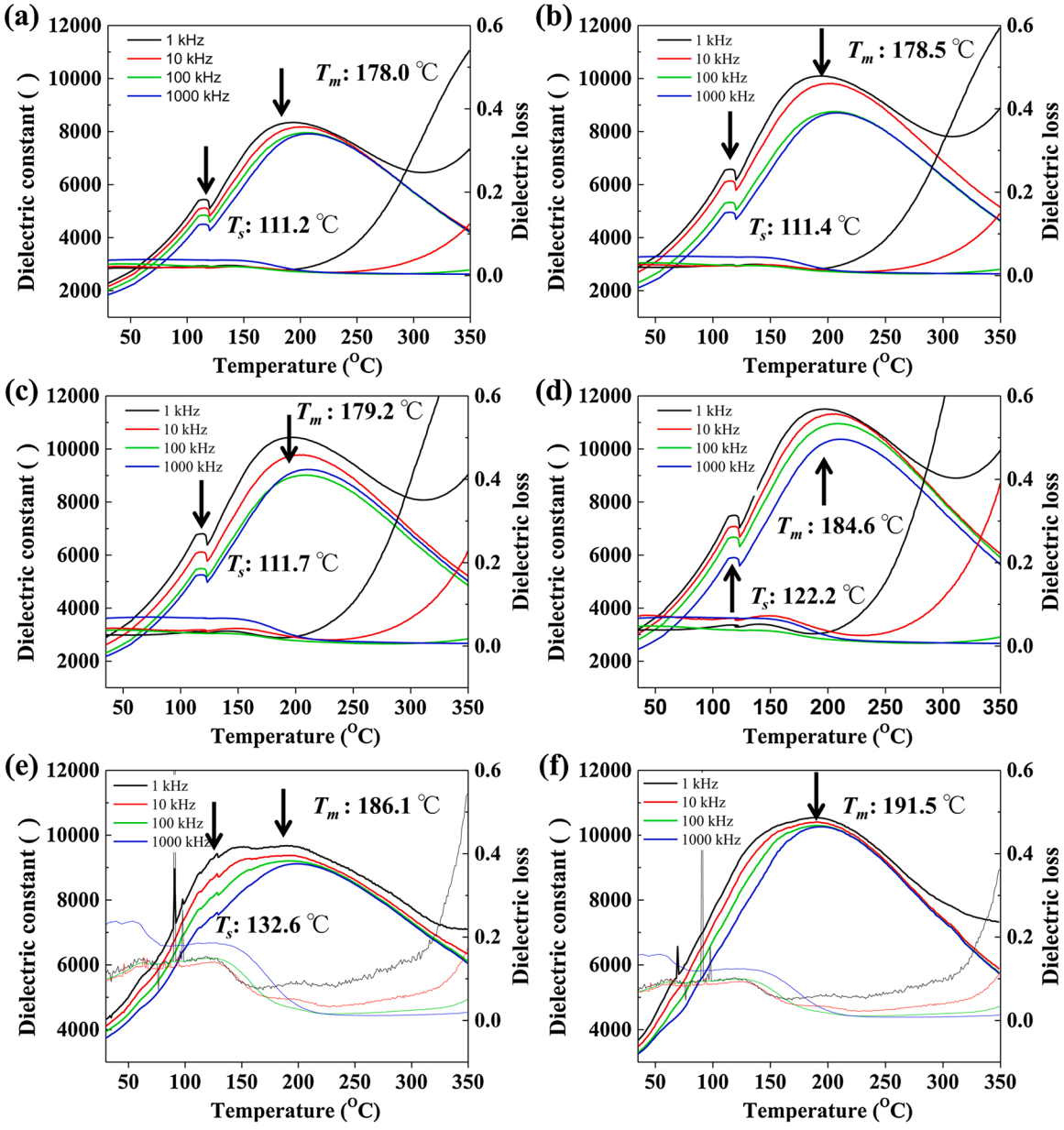

Fig. 3. Temperature dependence of dielectric constant and dielectric loss of the CB/BNT-ST composites with different CB contents: (a) BNT-ST, (b) 0.05/BNT-ST, (c) 0.10/BNT-ST, (d) 0.15/BNT-ST, (e) 0.20/BNT-ST and (f) 0.25/BNT-ST.

thermal evolution in the polar nano-region. Because the dielectric loss also increased with CB content, it was necessary to optimize the CB content in the CB/BNT-ST ceramics.

The CB/BNT-ST ceramics with different CB contents showed typical polarization–electric field (*P–E*) hysteresis loops and butterfly-shaped strain–electric field (*S–E*) curves at room temperature, as shown in Fig. 4. The polarization maximum (P_{max}), remanent polarization (P_r), coercive field (E_c), and strain calculated based on Fig. 4 are shown in Fig. S2 and Table S3. The P_{max} and strain values gradually increased with CB content, with maximum values of 40.02 μC/cm^2 and 0.25%, respectively, measured for the 0.10/BNT-ST ceramic. This is mainly because the tetragonality (c/a) determined based on the XRD results in Fig. 1 increased with CB content. In general, the best piezoelectric properties are exhibited in the morphotropic phase boundary (MPB) region, where rhombohedral and tetragonal phases coexist in BNT-ST–based piezoelectric ceramics. [32] However, an increase in the CB content may increase the tetragonality, resulting in a change in the MPB region, and thus the maximum P_{max} and strain were observed at a CB content of 10 wt%. Furthermore, because the maximum relative density of 99.99% was observed at a CB content of 10 wt% according to the SEM analysis shown in Fig. 2, the best piezoelectric performance was observed for the 0.10/BNT-ST ceramic. On the other hand, the P_r and E_c values decreased with increasing CB content because of the increasing number of free electrons in the piezoelectric ceramic.

The piezoelectric response amplitude loops and hysteresis phase loops of the CB/BNT-ST ceramics with different CB contents were investigated by scanning the axial DC bias from −10 to +10 V using piezoelectric force microscopy (PFM), as shown in Fig. 5. Typical butterfly-shaped amplitude loops and square hysteresis phase loops were observed for all the CB/BNT-ST ceramics, indicating a ferroelectric switching effect under an applied bias. [33]

The phase changes in the hysteresis phase loops were approximately 180 °, and the effective piezoelectric coefficients (d^*_{33}) calculated from the amplitude loops were 72 pm/V for BNT-ST, 74 pm/V for 0.05/BNT-ST, 76 pm/V for 0.10/BNT-ST, 76 pm/V for 0.15/BNT-ST, 76 pm/V for 0.20/BNT-ST, and 75 pm/V for 0.25/BNT-ST. Although the d^*_{33} values were improved by the addition of CB, a maximum d^*_{33} of approximately 76 m/V was observed in the 0.10/BNT-ST, 0.15/BNT-ST, and 0.20/BNT-ST ceramics. For the ceramics with excess CB, the piezoelectric performance seemed to degrade.

Table 1 shows the piezoelectric coefficients of all the CB/BNT-ST ceramics. The piezoelectric constant (d_{33}) was measured using a d_{33} meter, and the piezoelectric voltage coefficient (g_{33}), electromechanical coupling factor for thickness (K_t), planar electromechanical coupling factor (K_p), and quality factor (Q_m) were calculated based on Fig. 3. The overall piezoelectric coefficients gradually increased with CB content, and the maximum values of d_{33} (177.8 pC/N), g_{33} (27.4 mV/mN), K_p (38.16%), K_t (15.48%), and Q_m (36.26%) were measured for the 0.10/BNT-ST ceramic, similar to the results of the *P–E* and *S–E* analyses. It is believed that piezoelectricity can be diluted by free electrons blocking the polarization of the piezoelectric ceramic matrix due to excessive electrical conductivity. [21] In this regard, the CB content that afforded the CB/BNT-ST ceramic with the optimal piezoelectric performance was 10 wt%.

3.2. Optimization of PEHM performance

Based on the optimized CB content of 10 wt%, flexible CB/BNT-ST piezoelectric nanofibers were prepared by an electrospinning process. As shown by the FE-SEM images in Fig. 6(a), a uniform microstructure was observed for all the nanofibers, and the average diameters of the BNT-ST nanofibers and CB/BNT-ST nanofibers were approximately 230 and 375 nm, respectively. Furthermore, based on the TOPO image measured at a voltage of 10 V using PFM, the CB/BNT-ST nanofibers were thicker than the BNT-ST nanofibers, as shown in Fig. 6(b). This is because the viscosity of the precursor solution for the electrospinning process increased with the addition of CB nanoparticles. Fig. 6(b) also shows the typical butterfly-shaped amplitude loops and square hysteresis phase loops of both the BNT-ST and CB/BNT-ST nanofibers. The d^*_{33} values of the BNT-ST and CB/BNT-ST nanofibers were 61 and 66 pm/V, respectively. Although d^*_{33} of 66 pm/V for the CB/BNT-ST nanofibers is lower than that of the CB/BNT-ST ceramic powders (76 pm/V) due to compositing with a polymer, an improvement effect upon CB addition was similarly observed in the nanofibers. Typical *P–E* hysteresis loops and butterfly-shaped *S–E* curves were observed for both the BNT-ST and CB/BNT-ST nanofibers, as shown in Fig. 6(c). The P_{max} (18.1 μC/cm^2) and strain (0.12%) values of the CB/BNT-ST nanofibers were improved compared with P_{max} (14.36 μC/cm^2) and strain (0.09%) of the BNT-ST nanofibers, while P_r (10.71 μC/cm^2) and E_c (0.38 kV/mm) of the CB/BNT-ST nanofibers decreased compared with P_r (11.79 μC/cm^2) and E_c (0.71 kV/mm) of the BNT-ST nanofibers. These phenomena show that the relaxor properties were strengthened and the piezoelectric properties were greatly improved by the addition of CB.

PEHMs were manufactured using the BNT-ST and CB/BNT-ST nanofibers with an optimized interdigitated electrode structure, [25] and the single PEHMs were serially connected in a *z*-axis array. In both the BNT-ST nanofiber–based PEHM and CB/BNT-ST nanofiber–based PEHM, as the number of series-connected PEHMs increased, the output

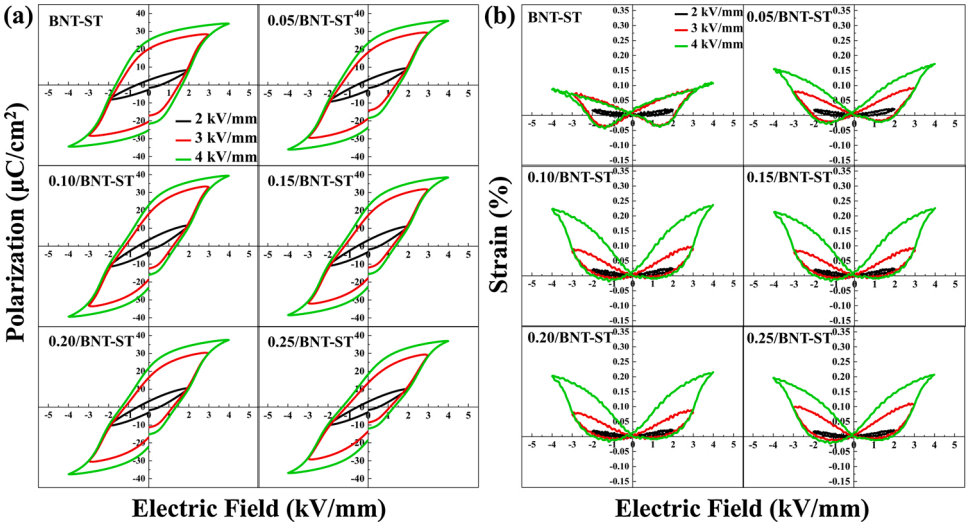

Fig. 4. (a) *P–E* hysteresis loops and (b) *S–E* curves of the CB/BNT-ST ceramics with different CB contents.

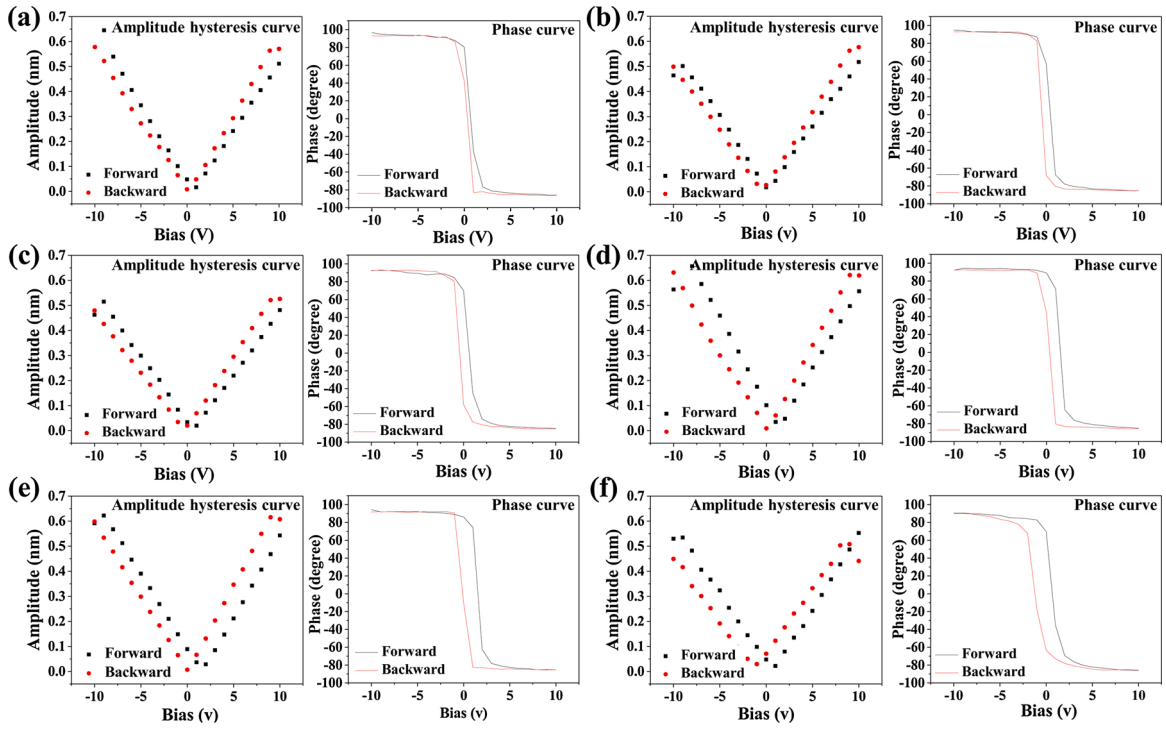

Fig. 5. Amplitude hysteresis curves and phase curves of the CB/BNT-ST ceramics with different CB contents: (a) BNT-ST, (b) 0.05/BNT-ST, (c) 0.10/BNT-ST, (d) 0.15/BNT-ST, (e) 0.20/BNT-ST and (f) 0.25/BNT-ST.

Table 1
Calculated d_{33}, g_{33}, K_p, K_t, and Q_m values of the CB/BNT-ST ceramics with different CB contents.

	d_{33} (pC/N)	g_{33} (mV/mN)	K_p (%)	K_t (%)	Q_m (%)
BNT-ST	165.2	21.5	29.21	12.58	27.25
0.05/BNT-ST	172.3	25.9	36.45	14.62	33.58
0.10/BNT-ST	177.8	27.4	38.16	15.48	36.26
0.15/BNT-ST	175.2	27.1	37.40	15.18	31.25
0.20/BNT-ST	173.6	26.9	35.17	14.09	30.59
0.25/BNT-ST	172.2	26.2	32.96	13.44	29.89

voltage and current gradually increased, as shown in Fig. 7. In the case of the PEHM with three module layers ($N = 3$), an output voltage of 6.4 V, current of 1.3 nA were observed at the load resistance of 5 MΩ for the BNT-ST nanofiber–based PEHM, while an output voltage of 10.1 V, current of 2.02 nA were observed at the load resistance of 5 MΩ for the CB/BNT-ST nanofiber–based PEHM. In other words, because the basic piezoelectric characteristics were greatly improved by the addition of CB with its high electrical conductivity, the piezoelectric energy harvesting performance, especially the current, was greatly improved for the PEHM with the CB/BNT-ST nanofibers instead of the BNT-ST nanofibers. As the number of series-connected PEHMs increased, the output performance also improved, but if more than four were connected, the module was too thick, making it difficult to apply a bending motion for energy generation. For this reason, the number of connected PEHMs was optimized to three.

3.3. Optimization of TEHM performance

The TEHM was manufactured based on a book-shaped structure with micropatterned polydimethylsiloxane (PDMS), with an aluminum electrode on one side and the CB/BNT-ST nanofibers with a metal mesh electrode on the other side. The operating mechanisms of the book-shaped TEHM according to the pressing–releasing mode, which are illustrated in Fig. S3, can be explained based on the coupling effects of contact electrification and electrostatic induction. The TEHM has sufficient separation between PDMS and the CB/BNT-ST nanofiber sheets in the initial state, and thus there is no electron movement. In the (I) pressing step, where the TEHM starts to be pressed by an external force, negative charges collect on the CB/BNT-ST surface because the electrons move from the PDMS layer to the CB/BNT-ST layer based on contact electrification according to electronegativity. In the (II) pressed step, the PDMS layer and CB/BNT-ST nanofiber layer come into complete contact and reach an equilibrium state, where each layer is electrically neutral. When the PDMS layer and CB/BNT-ST nanofiber layer are released in the (III) releasing step, the electrical neutrality of each layer is not maintained, and the tendency to maintain electrical neutrality causes current flow due to electrostatic induction in the opposite direction from that in the (I) pressing step. In the (Ⅳ) completely released state, the PDMS layer and CB/BNT-ST nanofiber layer are again in an electrically neutral state.

Based on the above operating mechanisms, the output voltage and current of the CB/BNT-ST nanofiber–based TEHM were analyzed according to the triboelectric area and compared with those of the BNT-ST nanofiber–based TEHM, as shown in Fig. 8. In both the BNT-ST nanofiber–based TEHM and CB/BNT-ST nanofiber–based TEHM, the output voltage and current gradually increased with the triboelectric area. This is because the generated triboelectric energy generally increases with the contact area. For the TEHMs with a triboelectric area of 5 cm (width) × 5 cm (length), output voltages of 384 and 394 V, currents of 77 and 131 μA were observed for the BNT-ST nanofiber–based TEHM and CB/BNT-ST nanofiber–based TEHM, respectively. Furthermore, the load resistance with the maximum output power were the 5 MΩ for the BNT-ST nanofiber–based TEHM and the 3 MΩ for the CB/BNT-ST nanofiber–based TEHM. In other words, with the addition of CB, while the output voltage increased by approximately 2.6%, the output current increased significantly to 70.1%. This increase in output current seems to be due to the increased surface energy difference between PDMS and the nanofibers with the addition of CB, as shown in Fig. S4. The surface energies of PDMS, BNT-ST nanofibers, CB/BNT-ST nanofibers, and CB were measured as 5.7, 5.1, 4.8, and 4.5 eV, respectively. With the

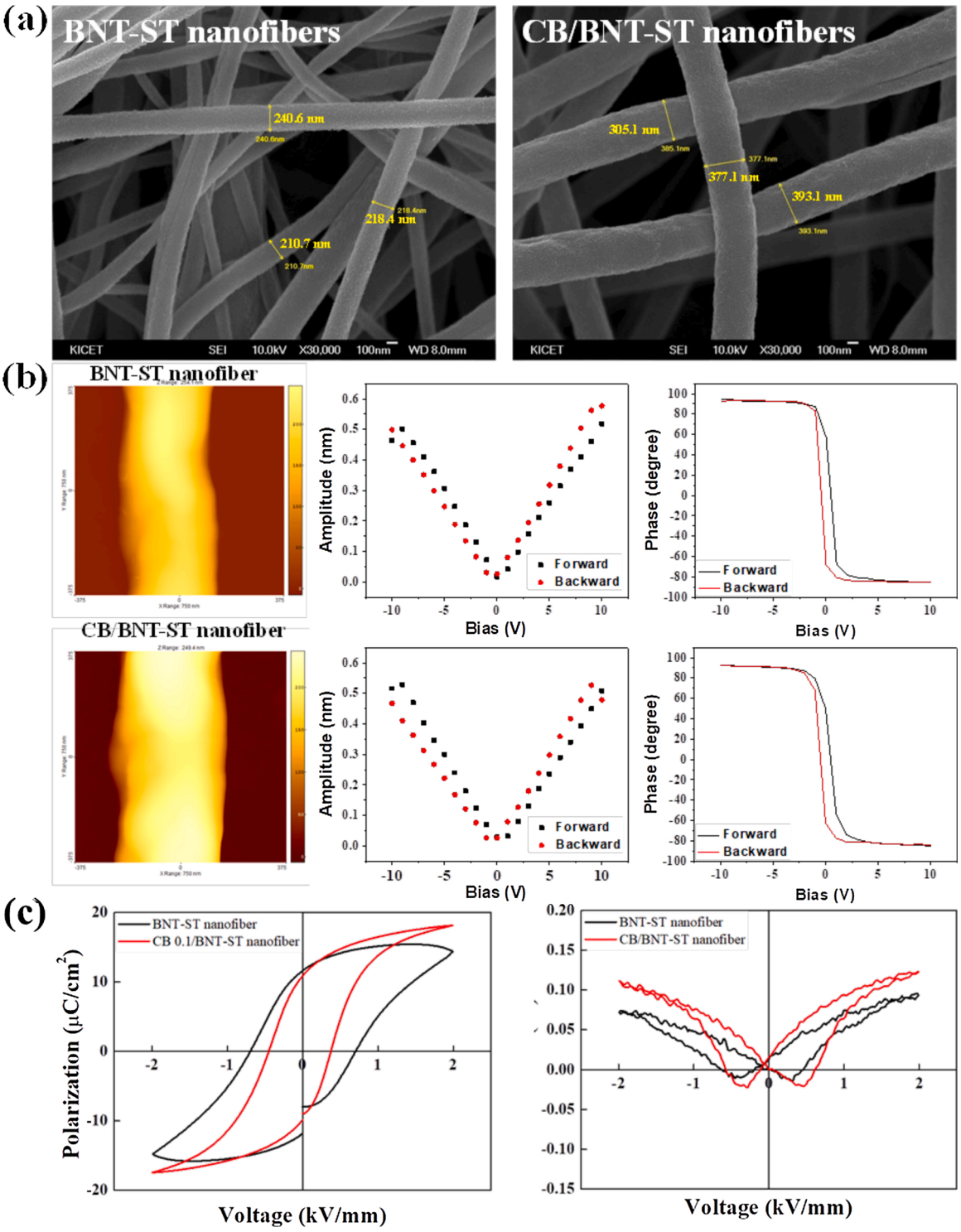

Fig. 6. (a) FE-SEM images, (b) PFM results, and (c) *P–E* and *S–E* hysteresis curves of the BNT-ST and CB/BNT-ST nanofibers.

addition of CB with its high conductivity, the surface energy of CB/BNT-ST was lowered, and the surface energy difference between PDMS and the CB/BNT-ST nanofibers became greater than 0.9 eV. It is believed that the triboelectric energy harvesting performance of the CB/BNT-ST nanofiber–based TEHM was greatly enhanced by improving the electron mobility based on this large surface energy difference. Furthermore, although the output performance was also improved as the triboelectric area of the TEHM increased, the triboelectric area of the TEHMs was optimized to 5 cm × 5 cm because of the size of the

3.4. Optimization of all-in-one HEHM performance

An all-in-one HEHM was manufactured by fitting PEHMs at both ends of the book-shaped TEHMs and connecting multiple layers to maximize the output power, as shown in the inset images in Fig. 9(b). The energy from the all-in-one HEHM was individually or integrally harvested from each individual PEHM and TEHM by performing opening and closing movements at a uniform speed (constant frequency). The book-shaped structure of the all-in-one HEHM has various advantages, such as ease and simplicity of multi-module manufacturing, and the

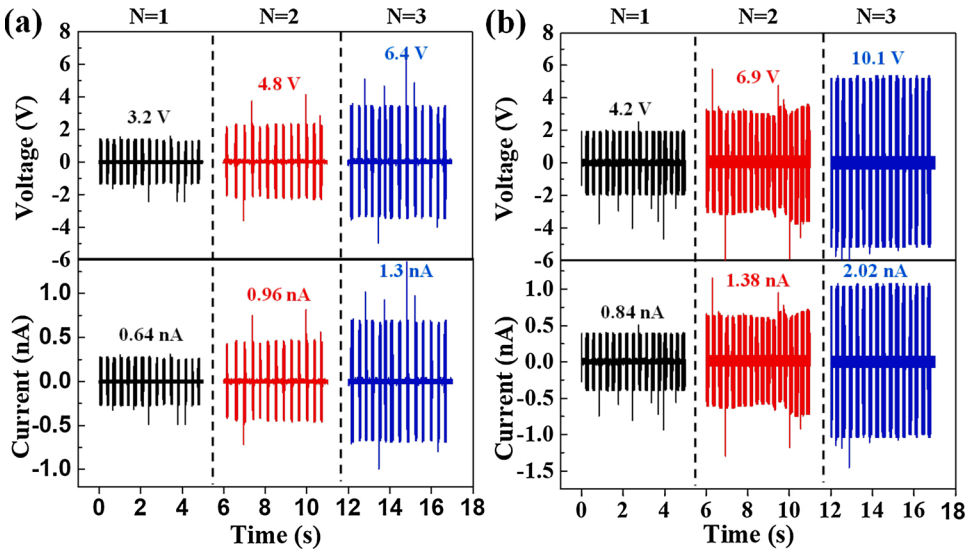

Fig. 7. Output voltage and current of the (a) BNT-ST nanofiber–based PEHM and (b) CB/BNT-ST nanofiber–based PEHM according to the number of modules.

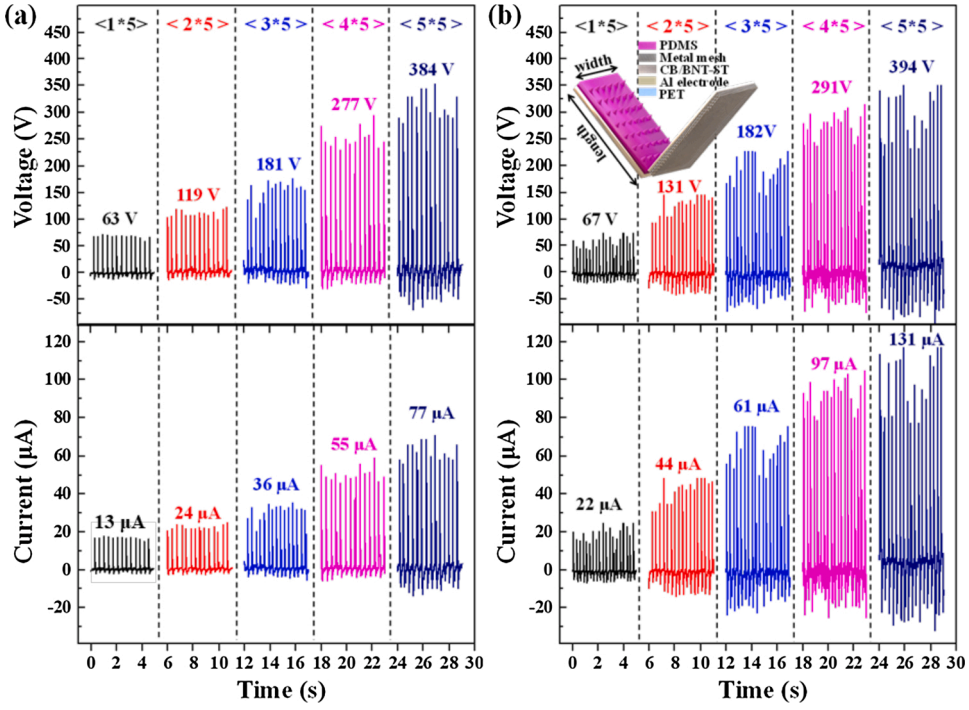

Fig. 8. Output voltage and current of the (a) BNT-ST nanofiber–based TEHM and (b) CB/BNT-ST nanofiber–based TEHM according to the triboelectric area.

reliability is secured based on quantitative evaluation using a bending machine. Fig. 9(a) shows that with increasing bending frequency from 1 to 5 Hz, although the output voltage of the all-in-one HEHM remained similar at approximately 388 V, the output current was significantly improved from 133 to 215 μA. In other words, when the contact speed and thus bending frequency increased, there was no obvious change in the output voltage, which simply depends on the amount of charge transferred, but the output current increased significantly. This is because the higher the frequency is, the shorter the contact time, which shortens the duration of the current peak and results in more active movement of free electrons in the layer. [34] The output voltage and current of the all-in-one HEHM according to the number of connected modules were measured at a bending frequency of 5 Hz, as shown in Fig. 9(b). The single HEHM (HEHM 1) showed an output voltage of 389 V, output current of 216 μA at the load resistance of 1.8 MΩ. Furthermore, the output voltage remained almost the same even after bending operations were performed more than 10,000 times, as shown in Fig. S5, illustrating the high durability of the module. HEHM 3, which consisted of three connected HEHMs, showed an improved output voltage (587 V), current (326 μA) at the load resistance of 1.8 MΩ, and HEHM 5 consisting of five connected HEHMs showed the highest voltage of up to 1043 V, highest current of 579 μA at the load resistance of 1.8 MΩ. This enhanced energy harvesting performance, especially the greatly improved output current, is expected to expand the applicability of this HEMH and generate energy suitable for applications by controlling the bending speed and number of modules.

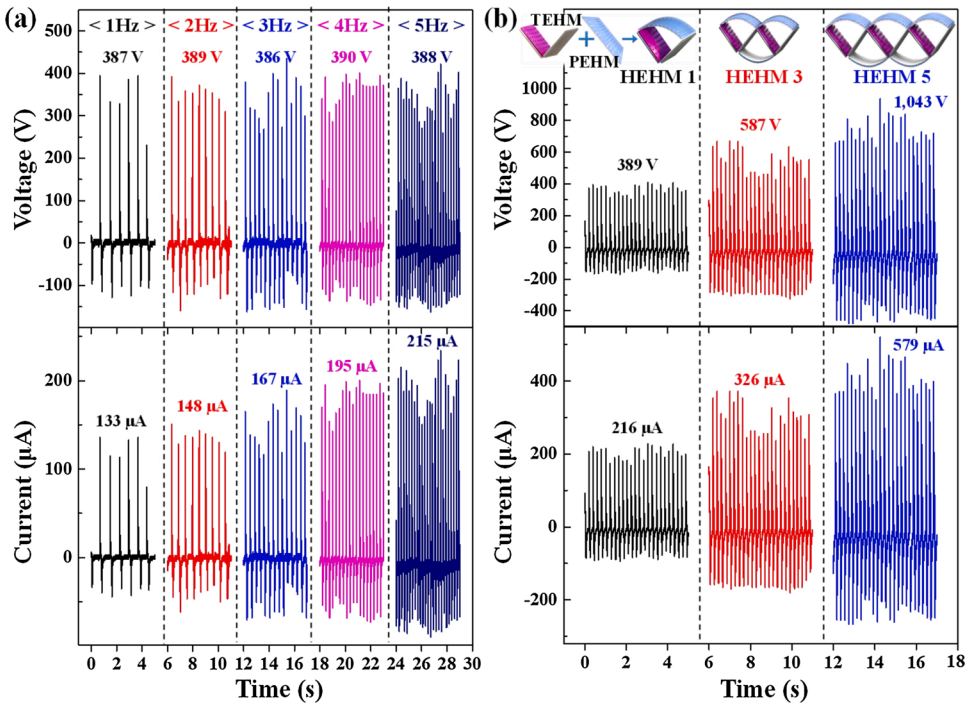

Fig. 9. Output voltage and current of all-in-one HEHMs according to the (a) bending frequency and (b) number of connected modules.

3.5. Simulated energy harvesting experiments

To use the all-in-one HEHM as an eco-friendly energy source in an actual situation, the harvested energy would usually be used after charging a capacitor to provide reliable power to the device. The voltage charged to a 1.0 μF capacitor using energy harvested from a PEHM, TEHM, and HEHM was measured for 100 s, as shown in Fig. 10(a). The PEHM could not fully charge the 1.0 μF capacitor in 100 s, while the TEHM and HEHM required 40 and 25 s to fully charge the capacitor to 25 V, respectively. In other words, in the all-in-one HEHM, the TEHM

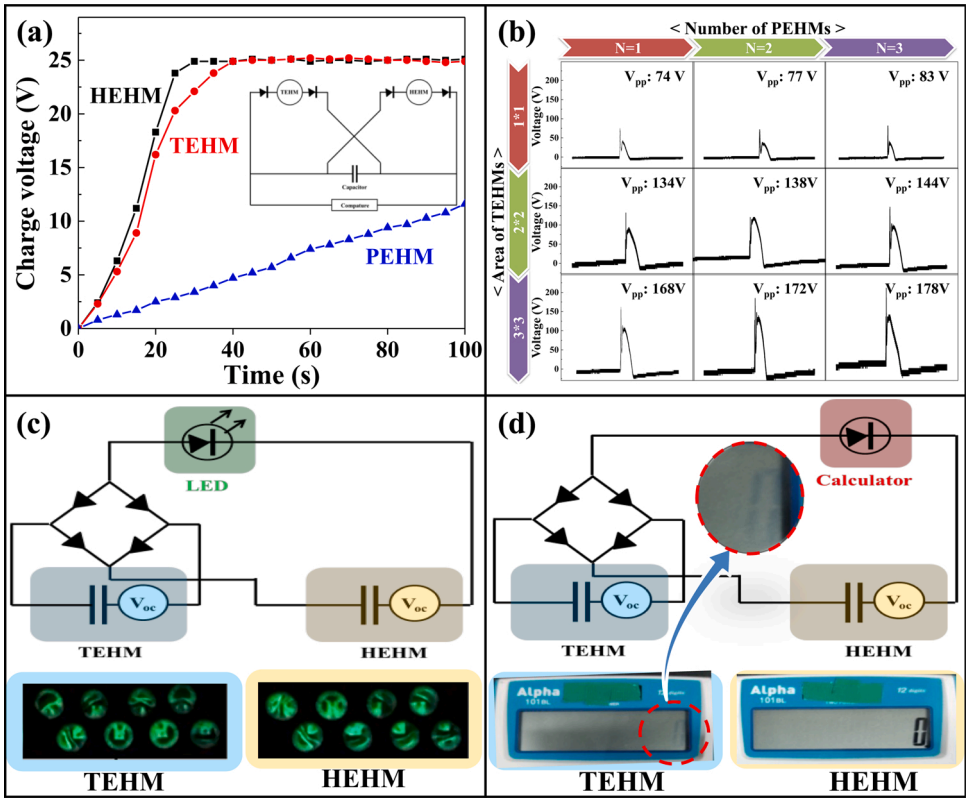

Fig. 10. (a) Charge curves of 1.0 μF capacitors, (b) output voltage according to the number of PEHMs and area of TEHMs, (c) lighting results of eight LED bulbs using TEHMs and HEHMs, and (d) operating results of an electronic calculator using TEHMs and HEHMs.

plays a major role in energy generation, while the PEHM improves the charging speed. By applying the easy-to-manufacture advantage of multiple modules of the book-shaped HEHM, the output voltage according to the number of PEHMs and the area of the TEHM were observed, as shown in Fig. 10(b). The output voltage increased with the number of PEHMs and the area of the TEHMs. These results demonstrate that the amount of harvested energy can be controlled according to the needs of the actual situation. To confirm whether a hybrid all-in-one structure of PEHMs and TEHMs is required, we compared and analyzed the energy harvesting performance of the TEHMs and all-in-one HEHM in simulated energy harvesting experiments of lighting LED bulbs and operating an electronic calculator, as shown in Fig. 10(c) and (d), respectively. In lighting the LED bulbs, as shown in Fig. 10(c), both the TEHM and all-in-one HEHM were able to operate eight LED bulbs in real time without charging, but the light of the LED bulbs powered by the all-in-one HEHM was brighter and more uniform. Furthermore, in the real-time operation of an electronic calculator, as shown in Fig. 10(d), the calculator powered by the TEHM had faint numbers on the LCD screen owing to the insufficient power supply, while the calculator powered by the all-in-one HEHM displayed clear numbers on the LCD screen. In other words, although most of the voltage is generated by the TEHM in the all-in-one HEHM, because the PEHM is hybridized, a higher voltage and current are supplied more stably, and thus it is believed that small electronic devices can be operated more stably. These simulated energy harvesting experiments confirmed that by improving the current with the addition of a small amount of conductive material and optimizing the structure of the module, the book-shaped all-in-one HEHM could be applied as an environmentally friendly energy harvester for small device operation.

4. Conclusions

A book-shaped all-in-one HEHM was manufactured by fitting PEHMs at both ends of book-shaped TEHMs and connecting multiple layers. To improve the output performance, especially the output current, flexible piezoceramic nanofibers composited with a small amount of high-conductivity CB were used in both the PEHM as a flexible piezoelectric material and the TEHM as a contact electrification material. Furthermore, the module structure was designed such that it is easy and simple to manufacture multiple layers and quantitatively evaluate the output performance. In this regard, the individual modules showed high output voltages and currents of 10.1 V and 2.02 nA for the PEHM and 391 V and 130 μA for the TEHM, respectively, and the integrated modules in the book-shaped all-in-one HEHM showed a high voltage and current of 1043 V and 579 μA, respectively. In the simulated energy harvesting experiments using the all-in-one HEHM, charging of a 1.0 μF capacitor was completed in 25 s, and eight LED light bulbs or an electronic calculator could be clearly operated in real time without charging. This work provides new insights into the design and application of all-in-one HEHMs as next-generation eco-friendly flexible energy sources.

Declaration of Competing Interest

The authors report no declarations of interest.

Acknowledgements

This work was supported by the Industrial Fundamental Technology Development Program (2021R1A2C2010145, Development of flexible all-in-one piezo-triboelectric energy harvester module with high performance of over 250 V based on lead-free piezoelectric ceramic nanofibers) funded by the National Research Foundation(NRF) of Korea.

Appendix A. Supplementary data

Supplementary material related to this article can be found, in the online version, at doi:https://doi.org/10.1016/j.jeurceramsoc.2021.11.047.

References

[1] N. Sezer, M.A. Koç, Comprehensive Review on the State-of-the-Art of Piezoelectric Energy Harvesting, Nano Energy 80 (2021), 105567.
[2] M.M. Farid, A.M. Khudhair, S.A.K. Razack, S. Al-Hallaj, A Review on Phase Change Energy Storage: Materials and Applications, Energy Convers, Managem. 45 (2004) 1597–1615.
[3] O. Paish, Small Hydro Power: Technology and Current Status, Renewable Sustainable Energy Rev. 6 (2002) 537–556.
[4] I.G. Bryden, T. Grinsted, G.T. Melville, Assessing the Potential of a Simple Tidal Channel to Deliver Useful Energy, Appl. Ocean. Res. 26 (2004) 198–204.
[5] Z. Yang, Y.Q. Wang, L. Zuo, J. Zu, Introducing Arc-Shaped Piezoelectric Elements into Energy Harvesters, Energy Convers. Manage. 148 (2017) 260–266.
[6] Z.L. Wang, J. Chen, L. Lin, Progress in Triboelectric Nanogenerators As a New Energy Technology and Self-Powered Sensors, Energy Environ. Sci. 8 (2015) 2250–2282.
[7] Q. Xu, J. Wen, Y. Qin, Development and Outlook of High Output Piezoelectric Nanogenerators, Nano Energy 86 (2021), 106080.
[8] A. Yar, High Performance of Multi-Layered Triboelectric Nanogenerators for Mechanical Energy Harvesting, Energy 222 (2021), 119949.
[9] C. Zhao, Q. Zhangm, W. Zhang, X. Du, Y. Zhang, S. Gong, K. Ren, Q. Sun, Z. L. Wang, Hybrid piezo/triboelectric nanogenerator for highly efficient and stable rotation energy harvesting, Nano Energy 57 (2019) 440–449.
[10] X. Cao, Y. Xiong, J. Sun, X. Zhu, Q. Sun, Z.L. Wang, Piezoelectric Nanogenerators Derived Self-Powered Sensors for Multifunctional Applications and Artificial Intelligence, Adv. Funct. Mater. (2021), 2102983.
[11] J. Huang, X. Yang, J. Yu, J. Han, C. Jia, M. Ding, J. Sun, X. Cao, Q. Sun, Z.L. Wang, A universal and arbitrary tactile interactive system based on self-powered optical communication, Nano Energy 69 (2020), 104419.
[12] Y. Qi, J. Kim, T.D. Nguyen, B. Lisko, P.K. Purohit, M.C. McAlpine, Enhanced Piezoelectricity and Stretchability in Energy Harvesting Devices Fabricated from Buckled PZT Ribbons, Nano Lett. 11 (2021) 1331–1336.
[13] X. Niu, W. Jia, S. Qian, J. Zhu, J. Zhang, X. Hou, J. Mu, W. Geng, J. Cho, J. He, X. Chou, High-Performance PZT-Based Stretchable Piezoelectric Nanogenerator, ACS Sustainable Chem. Eng. 7 (2018) 979–985.
[14] T. Karaki, K. Yan, T. Miyamoto, M. Adachi, Lead-Free Piezoelectric Ceramics with Large Dielectric and Piezoelectric Constants Manufactured from $BaTiO_3$ Nano-Powder, Jpn. J. Appl. Phys. 46 (2007) L97.
[15] K.-L. Park, S. Xu, Y. Liu, G.-T. Hwang, S.-J.L. Kang, Z.L. Wang, K.J. Lee, Piezoelectric $BaTiO_3$ Thin Film Nanogenerator on Plastic Substrates, Nano Lett. 10 (2010) 4939–4943.
[16] J.H. Lee, H. Ryu, T.-Y. Kim, S.-S. Kwak, H.-J. Yoon, T.-H. Kim, W. Seung, S.-W. Kim, Thermally Induced Strain-Coupled Highly Stretchable and Sensitive Pyroelectric Nanogenerators, Adv. Energy Mater. 5 (2015), 1500704.
[17] A. Datta, Y.S. Choi, E. Chalmers, C. Ou, S. Kar-Narayan, Piezoelectric Nylon-11 Nanowire Arrays Grown by Template Wetting for Vibrational Energy Harvesting Applications, Adv. Funct. Mater. 27 (2017), 1604262.
[18] S.H. Ji, J.H. Cho, J.-H. Paik, J. Yun, J.S. Yun, Poling Effects on the Performance of a Lead-Free Piezoelectric Nanofiber in a Structural Health Monitoring Sensor, Sens. Actuators A 263 (2017) 633–638.
[19] Y. Zhang, Z. Liu, J. Yu, M. Fan, X. Ji, B. Sun, P. Hu, Optimizing the Dielectric Energy Storage Performance in P(VDF-HFP) Nanocomposite by Modulating the Diameter of PZT Nanofibers Prepared via Electrospinning, Compos. Sci. Technol. 184 (2019), 107838.
[20] H.-Y. Song, H.-C. Kim, C.-Y. Kang, H.-J. Kim, S.-J. Yoon, D.-Y. Jeong, Multilayer piezoelectric energy scavenger for large current generation, J. Electroceram. 23 (2009) 301–304.
[21] S. Mishra, L. Unnikrishnan, S.K. Nayak, S. Mohanty, Advances in Piezoelectric Polymer Composites for Energy Harvesting Applications: A Systematic Review, Macromol. Mater. Eng. 340 (2018) 1800463–1800488.
[22] S.H. Ji, W. Lee, J.S. Yun, All-in-One Piezo-Triboelectric Energy Harvester Module Based on Piezoceramic Nanofibers for Wearable Devices, ACS Appl. Mater. Interfaces 12 (2020) 18609–18616.
[23] H. Gong, Z. Li, Y. Zhang, R. Fan, Piezoelectric and Dielectric Behavior of 0-3 Cement-Based Composites Mixed with Carbon Black, J. Eur. Ceram. Soc. 29 (2009) 2013–2019.
[24] N. Jayababu, D. Kim, ZnO Nanorods@Conductive Carbon Black Nanocomposite Based Flexible Integrated System for Energy Conversion and Storage Through Triboelectric Nanogenerator and Supercapacitor, Nano Energy 82 (2021), 105726.
[25] S.H. Ji, J.S. Yun, Optimization of a Flexible Piezoelectric Module Structure Based on a Lead-Free Piezoceramic Embedded in Nanofiber Composites, Mech. Syst. Signal Process. 136 (2020), 106447.
[26] F. Yang, Z. Zhang, Y. Han, K. Du, Y. Lai, J. Li, TiO_2/Carbon Hollow Spheres As Anode Materials for Advanced Sodium Ion Batteries, Electrochim. Acta 178 (2015) 871–876.
[27] X. Liu, X. Tam, Giant Strains in Non-Textured $(Bi_{1/2}Na_{1/2})TiO_3$-Based Lead-Free Ceramics, Adv. Mater. 28 (2016) 574–578.
[28] W. Photankham, H. Wattansarn, T. Seetawan, Effect of Carbon Black Added $BaTiO_3$ on Dielectric and Ferroelectric Properties, Int. J. Recent Eng. Res. Dev. 2 (2017) 94–98.

[29] T. Seetawan, W. Photankham, H. Wattansarn, S. Phewphong, Influence of Nano Carbon Black Added $BaTiO_3$ on Physical and Dielectric Properties, Mater. Today: Proc. 4 (2017) 6472–6477.

[30] P. Zheng, J.L. Zhang, Y.Q. Tan, C.L. Wang, Grain-Size Effects on Dielectric and Piezoelectric Properties of Poled $BaTiO_3$ Ceramics, Acta. Mater. 60 (2012) 5022–5030.

[31] W. Jo, S. Schaab, E. Sapper, L.A. Schmitt, H.-J. Kleebe, A.J. Bell, J. Rödel, On the Phase Identity and Its Thermal Evolution of Lead Free $(Bi_{1/2}Na_{1/2})TiO_3$-6 mol% $BaTiO_3$, J. Appl. Phys. 110 (2011), 074106.

[32] M. Afifi, A.O. Turky, M. Rasly, M.M. Rashad, J.A. Turner, Field-Induced Polarization Response and Energy Storage Behavior of Lead-Free BNT-BKT-SZ Films, Ceram. Int. 46 (2020) 26061–26068.

[33] Y. Shi, S.Y. Wang, S. Ma, Y.L. Lei, H.L. Liu, X.L. Chen, W.F. Liu, Nanoscale Imaging of Ferroelectric Domain and Resistance Switching in Hybrid Improper Ferroelectric $Ca_3Ti_2O_7$ Thin Films, Phys. Lett. A 384 (2020), 126609.

[34] Z. Lin, Y. Wu, Q. He, C. Sun, E. Fan, Z. Zhou, M. Liu, W. Wei, J. Yang, An Airtight-Cavity-Structural Triboelectric Nanogenerator-Based Insole for High Performance Biomechanical Energy Harvesting, Nanoscale 11 (2019) 6802–6809.